Chapter 1

Modeling of Tire and Vehicle Dynamics

1.1. Introduction

A vehicle is a highly complex system bringing together a large number of mechanical, electronic and electromechanical elements. It has two primary subsystems that require kinematic motion descriptions. The first subsystem is the vehicle body, while the second is the tire, which, through its four occurrences in the vehicle system, are our means of generating force through contact with the road. Since these subsystems are rigidly interconnected by suspensions, we can deduce that they have kinematic relationships with one another. Hence, the overall vehicle motion is dependent on the kinematics of both subsystems.

To describe the vehicle movements, numerous measurements and mathematical formulations, also called vehicle models, representing the system behavior are required. The fineness degree of modeling depends on the desired objectives. For a simulator design, modeling efforts are concentrated on reproducing as precisely as possible the behavior of individual vehicle components. This approach has yielded, for example, exact descriptions of the wheel dynamics using the finite element method. Simulations of such models are computationally expensive and time-consuming. However, when it comes to real-time applications (vehicle motion reproduction system, vehicle controllers and so on), we have to make simplifications because of the limited calculation capacity.

In this book, the backbone for the vehicle-state estimators developed so far is a vehicle model that accurately describes all dynamics of interest, as simply as possible.

Vehicle dynamics has been widely studied for more than 60 years. Many references on this subject are available. We can refer to [GIL 92, JAZ 08, KIE 00, MIL 95, RAJ 06]. This chapter reviews the fundamental features of vehicle dynamics theory from the tire/road contact leading to the chassis movement with the focus on simplified-oriented modeling. First, the tire forces/moments are described, and then vertical, lateral and longitudinal vehicle behaviors are discussed. The different notations used in the following sections are given in Appendix 5.

1.2. Tire dynamics

Tires are the main vehicle components generating external forces that can be effectively manipulated to affect vehicle motions. Thus, they are crucial for vehicle dynamics, and consequently it is important to have a good understanding of tire mechanics. Actually, the pneumatic tires on a vehicle can create both longitudinal and lateral forces, allowing the car to accelerate/brake and to turn. The developed forces are the function of tire properties (material, tread pattern, tread depth, profile, etc.), the normal load on the tire and the velocities experienced by the tire. The relationship between these factors is extremely complex and nonlinear, and it is still subject to numerous research activities. Before introducing and analyzing some tire models, let us start by defining the tire efforts and moments.

1.2.1. *Tire forces and moments*

Unlike a rigid undeformable wheel, the tire does not make contact with the road at just one point. Instead, the tire on a vehicle deforms due to the vertical load on it, and makes contact with the road over a non-zero footprint area called the contact patch. The force the tire receives from the road is assumed to be at the center of the contact patch and can be decomposed along the three wheel axes. The lateral force, F_y, is the force along the Y axis, the longitudinal force, F_x, is the force along the X axis and the normal or vertical force, F_z, is the force along the Z axis. Similarly, the moment the tire receives from the road can be decomposed along the three axes. The moment along the Z axis, M_z, is called the aligning moment, the moment along the X axis, M_x, is called the overturning moment and the moment along the Y axis, M_y, is called the rolling moment. Figure 1.1 shows the tire dynamic variables set.

In the following, basic concepts related to vertical tire forces, F_z, longitudinal forces, F_x, lateral forces, F_y, the aligning moment, M_z, and road friction are discussed.

1.2.1.1. *Vertical/normal forces*

The weight of the vehicle contributes to the major part of the vertical forces F_{zij} on the tires, where $i \in \{1, 2\}$ represents the front or the rear tire and $j \in \{1, 2\}$ represents the left or the right tire. Longitudinal acceleration and deceleration forces

acting on the vehicle redistribute the vertical forces between the tires. For example, an acceleration of the vehicle causes the vertical forces on the front tires to decrease and the vertical forces on the rear tires to increase. A braking action increases the vertical forces on the front tires and decreases vertical forces on rear tires. During cornering, the vertical forces of the right and left tires on both the front and rear axle are different due to vehicle roll moment. This concept is illustrated in more detail in section 1.4.2.2. Accurate knowledge of each F_{zij} is fundamental when evaluating lateral and longitudinal tire forces generated through tire adhesion.

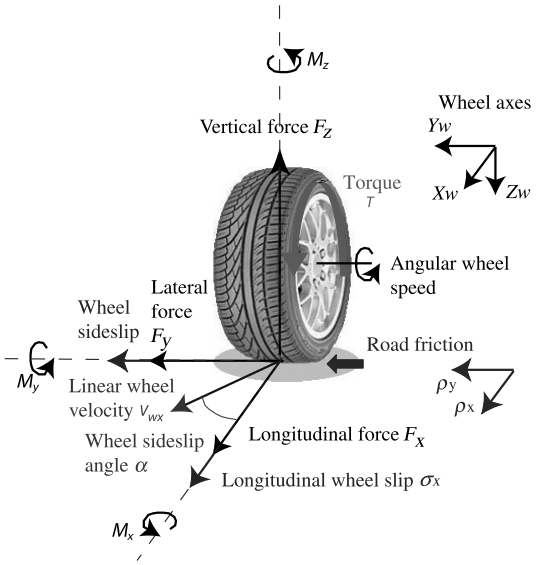

Figure 1.1. *Tire dynamic variables set*

1.2.1.2. *Longitudinal forces and longitudinal slip ratio*

In order to accelerate or brake, longitudinal friction forces must be developed between the tires and the ground in the tire footprint (see Figure 1.1). Experimental results have established that the longitudinal tire force generated by each tire depends on [GIL 92, RAJ 06]:

– the slip ratio (defined below);

– the vertical load on the tire;

– the friction coefficient of the tire–road interface (defined in section 1.2.2).

The difference between the actual longitudinal velocity at the wheel axle V_{wx} and the equivalent rotational velocity $R_{\text{eff}}w$ of the tire is called longitudinal slip, where w is the wheel rotational velocity and R_{eff} is the effective tire radius. In other words, longitudinal slip is equal to $(R_{\text{eff}}w - V_{wx})$.

The longitudinal slip ratio is defined as:

$$\begin{aligned} \sigma_x &= \frac{R_{\text{eff}} w - V_{wx}}{V_{wx}} \quad \text{during braking,} \\ \sigma_x &= \frac{R_{\text{eff}} w - V_{wx}}{R_{\text{eff}} w} \quad \text{during accelerating.} \end{aligned} \qquad [1.1]$$

Figure 1.2 shows the evolution of the longitudinal force with respect to the longitudinal slip ratio on the front right tire during a real vehicle movement. As can be seen from this figure, in the case where the longitudinal slip ratio is small, as it is during normal driving, the longitudinal tire force is found to be proportional to the slip ratio. However, if the longitudinal slip ratio is not small, the relation between the longitudinal slip ratio and the longitudinal force becomes nonlinear. More details concerning these concepts are provided in section 1.2.3 when dealing with the tire's model.

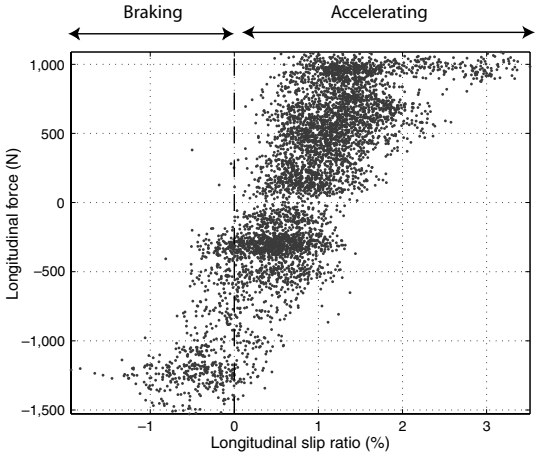

Figure 1.2. *Longitudinal force versus longitudinal slip ratio*

1.2.1.3. *Lateral forces and sideslip angle*

During a vehicle turn, a lateral force originates at the center of the tire that is in contact with the road, lies in the horizontal plane and is perpendicular to the direction in which the wheel is headed if no inclination or camber exists [MIL 95]. This is also called the side force.

A vehicle can turn because of the applied lateral tire forces. To transmit lateral forces, the tire must evade laterally. This means that the direction of the tire motion deviates from the wheel plane. The angle between the wheel linear velocity vector and the wheel plane is called the tire sideslip angle α (see Figure 1.1). Consequently,

the lateral force may be thought of as the result of the slip angle, or the slip angle as the result of the lateral force. Furthermore, the studies prove that the lateral force is also hugely affected by the vertical load applied to the tire and by the road friction [MIL 95, RAJ 06].

Figure 1.3 shows the lateral force variations with respect to the sideslip angles for the front right tire. This figure is constructed according to experimental data acquired during a real vehicle motion. It is clear that for small slip angles, the force profile can be defined by a linear region. As the slip angle continues to grow, the tire begins to saturate and reaches a nonlinear region of the tire curve. More explanations about these phenomena are given in section 1.2.3.

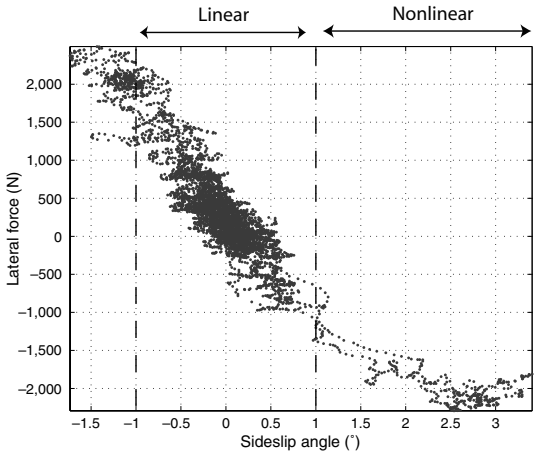

Figure 1.3. *Lateral force versus sideslip angle*

1.2.1.4. *Aligning moment*

Pneumatic tire self-aligning (or aligning) moment is primarily generated by two sources: the characteristics of the side deformation of a forward moving tire with non-zero slip angle and the steering geometry [WAN 07]. The resultant lateral force from the ground acts behind the wheel center in the ground plane as shown in Figure 1.4(a). Then, it forms a torque with tendency to align the wheel plane with the direction of wheel travel. The distance t_p is called pneumatic trail as shown in Figure 1.4(a).

Another contribution to the tire self-aligning moment is from the mechanical steering geometry, particularly the caster angle, which is the angular displacement, θ_c, between the tire steering axis and vertical direction as shown in Figure 1.4(b). The distance between the center of the tire–ground contact patch and the intersection point of the steering axis with the ground is called the mechanical trail, t_m, which is

determined by the steering geometry and tire dimensions. Therefore, the lateral force applied on the tire contact patch forms a torque against the steering direction.

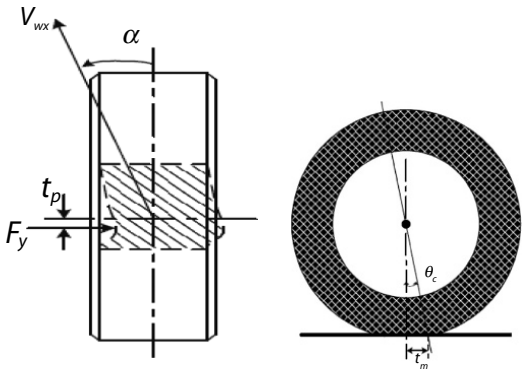

Figure 1.4. *Tire self-aligning moment characteristics*

In general, these two contributions add to yield the tire self-aligning moment as

$$M_z = F_y(t_p + t_m). \qquad [1.2]$$

A typical tire self-aligning torque moment as a function of the tire slip angle is shown in Figure 1.5. At small slip angle values, the self-aligning moment is associated with the slip angle linearly. However, as the slip angle becomes larger, the relationship becomes very nonlinear and the self-aligning moment peaks and then decreases dramatically at a large slip angle. The self-aligning moment helps the steered tire to return to its original position after a turn action and this is important for vehicle handling stability. It is the main torque acting against the steering actuation.

In addition to being connected with tire slip angle, self-aligning effects are also subject to other factors such as the tire normal force, the tire–road friction coefficient and the longitudinal force.

1.2.1.5. *Coupling effects between longitudinal and lateral tire forces*

In the above discussions on tire forces and moments, the coupling effects between the longitudinal and lateral tire forces were not introduced. However, it is very common that a tire experiences both longitudinal and lateral forces such as during accelerating/braking in a turn maneuver. The coupling effects between tire longitudinal and lateral forces are important in vehicle dynamics interpretation, especially when both tire longitudinal and lateral forces need to be utilized simultaneously.

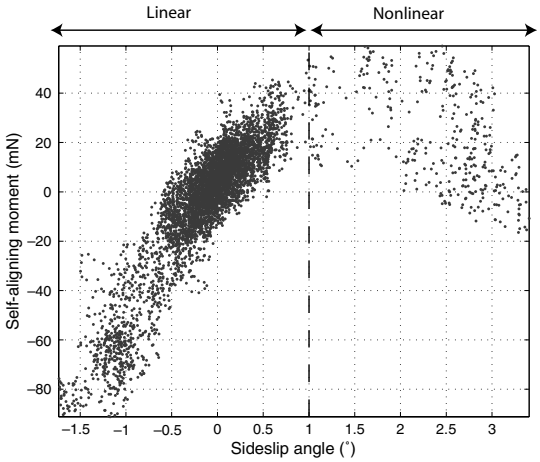

Figure 1.5. *Self-aligning torque versus sideslip angle*

In the presence of both the sideslip angle and slip ratio, it must be noted that the total vector sum of the force generated cannot exceed μF_z, where μ is the road friction defined in section 1.2.2. This is due to the fact that there is a limited amount of tire force that can be generated in the contact patch. The tire adhesion capability used for generating longitudinal tire force therefore limits how much lateral tire force can be generated in the contact patch, and vice versa. This combined force analysis is also called the *friction circle* concept (lateral force vs. longitudinal force) [GIL 92, SVE 07]. In section 1.2.3.2, a combined force model is represented. This model illustrates how the lateral tire force generation is affected by the presence of longitudinal tire force (from drive or brake forces).

1.2.2. *Tire–road friction coefficient*

Let F_x, F_y and F_z be the longitudinal, lateral and vertical forces acting on a tire, respectively. The normalized traction force for the tire, ρ, is defined as [RAJ 06]:

$$\rho = \frac{\sqrt{F_x^2 + F_y^2}}{F_z}. \qquad [1.3]$$

ρ can vary between 0 and a maximum value called the friction coefficient (μ). μ depends essentially on the tire characteristics and the road states. For example, dry road surfaces show normally a high μ, which results in safe driving on such surfaces. In contrast, in case of snow, due to frictional heating induced by sliding over the surface of the tire rubber, a thin water layer is generated, reducing the transmittable

force to the very low level of viscose sliding friction. This ends up in a low maximum friction coefficient. Average μ values for different road conditions can be summarized as in Table 1.1 [UCH 01].

Road condition	Approximated μ
Asphalt, dry	0.9–1.1
Concrete, dry	0.85–1
Asphalt, wet	0.5–0.8
Concrete, wet	0.5–0.8
Snow, packed	0.2–0.3
Ice	0.15–0.2

Table 1.1. *μ values as a function of road surface*

In [KIE 00], a model is discussed where the friction behavior of a tire is approximated with the normal load applied to it and with other parameters that depend on the tire's characteristics and the road surface (Burckhardt model). Such typical friction variation for a resultant slip of 10% can be illustrated as in Figure 1.6, where the vehicle speed is about 20 m/s, and the wheel contact force is around 4,500 N.

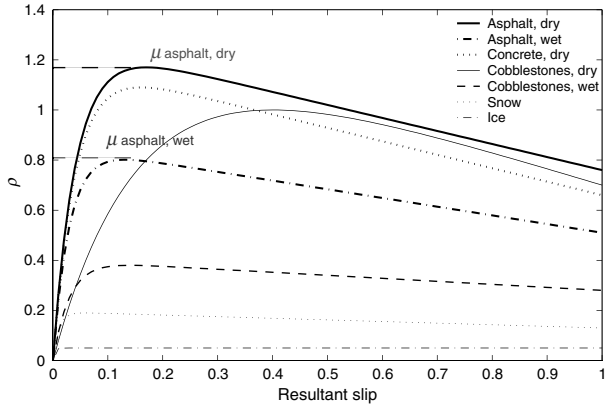

Figure 1.6. *Typical ρ curve for different road surfaces: the vehicle velocity about 20 m/s, and the wheel contact force around 4,500 N (figure deduced from [KIE 00])*

Note that some researchers refer to the normalized traction force, ρ, as the friction coefficient and to μ as the *maximum* friction coefficient. This study will, however, refer to ρ as the normalized traction force and to μ simply as the tire–road friction coefficient.

The normalized traction force ρ is decomposed into longitudinal and lateral components, ρ_x and ρ_y, respectively, in such a way that:

$$\rho = \sqrt{\rho_x^2 + \rho_y^2}, \qquad [1.4]$$

where ρ_x and ρ_y are defined and analyzed in the following.

1.2.2.1. *Normalized longitudinal traction force*

The normalized longitudinal traction force for the tire is defined as in [MIL 95]:

$$\rho_x(\sigma_x) = \frac{F_x}{F_z}. \qquad [1.5]$$

ρ_x is also called the mobilized longitudinal friction. Figure 1.7 represents ρ_x as a function of longitudinal slip ratio for different loads and for a given road. Analyzing this figure, we can deduce that the friction coefficient reaches a peak value, μ_x, before dropping to an almost steady-state value. It is also shown that the longitudinal friction coefficient falls as the load increases. Note that μ_x is also called the longitudinal friction coefficient, and it depends on the tire's characteristics and on the road surface.

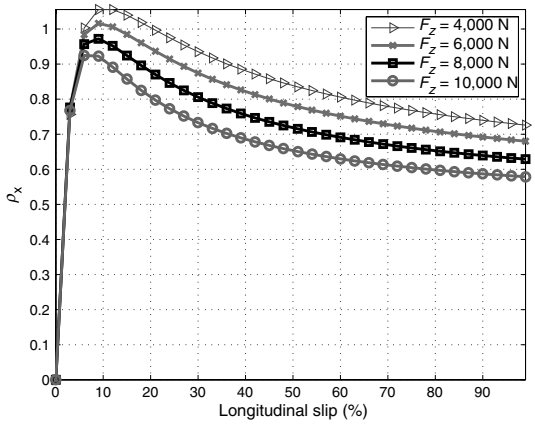

Figure 1.7. *Longitudinal friction coefficient versus longitudinal slip*

1.2.2.2. *Normalized lateral traction force*

The normalized lateral traction force for the tire is given by [MIL 95]:

$$\rho_y(\alpha) = \frac{F_y}{F_z}. \qquad [1.6]$$

It is obvious that ρ_y, also called the mobilized lateral friction, is a function of the sideslip angle. ρ_y varies between 0 and μ_y and is defined as the lateral friction

coefficient. Figure 1.8 shows the variation of ρ_y for different loads and for a given road. A closer investigation reveals that the mobilized lateral friction coefficient is normally higher for the lighter loads. This effect is called the *tire load sensitivity* [MIL 95]. Both the magnitude of the lateral force and its variation with normal load are important when analyzing the vehicle handling limits.

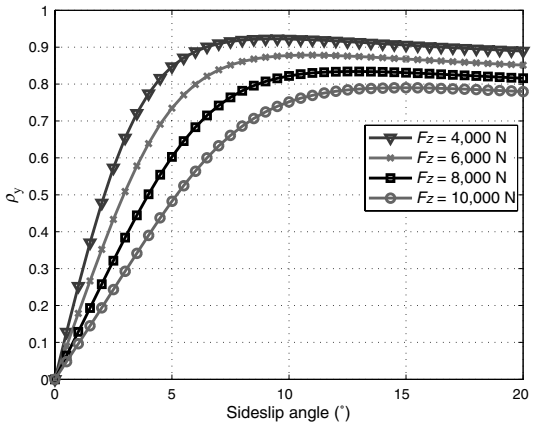

Figure 1.8. *Lateral friction coefficient versus slip angle*

1.2.3. *Quasi-static tire model*

The aim of a tire model is often to obtain a structure that fits measurement data well by an optimal choice of included parameters. It is very desirable to have some mathematical models for estimating the complex tire behaviors. In this field, significant research efforts have been developed over the past several decades. One of these methods is to use the construction data of a particular tire and/or finite element modeling. This is computationally expensive and difficult, but is commonly used in certain studies. However, for reasons of simplicity, more practical methods for general use are needed. They are often semi-empirical and empirical models, whose formulations are based on experimental data. In this context, there exist numerous tire models, varying from a simple proportional linear model to the so-called Magic formula model that is characterized by multiple empirical parameters. However, in practice, the exact shape and nuances of the tire curve are generally unknown.

In this chapter, three models are discussed: the Magic tire formula, the Dugoff and the linear models. They concern the steady-state relation between the slip and the developed tire force.

1.2.3.1. *Pacejka's magic tire model*

The best known and most widely used semi-empirical tire model is the so-called *Magic Tire* model proposed by Pacejka [PAC 87, PAC 97, PAC 02]. It is called semi-empirical because the model is based not only on measured data but also on structures that come from physical models. This model was developed as a joint venture between the Volvo Car Corporation and Delft University of Technology. The goal was to develop a tire model that could accurately describe the characteristics of longitudinal force, lateral force and self-aligning torque in pure and combined slip situations. According to Pacejka, the tire model should be:

– able to describe all steady-state tire characteristics;

– easily obtainable from measured data;

– physically meaningful; its parameters should characterize in some way the typifying quantities of the tire (this feature would make it possible to investigate the effect of changes of these quantities upon the handling and stability properties of the vehicle);

– compact and easy to use;

– able to contribute to a better understanding of tire behavior.

The basic formula for this model is:

$$y = D\sin[C\arctan\{Bx - E(Bx - \arctan Bx)\}], \qquad [1.7]$$

with

$$\begin{aligned} Y(x) &= y(x) + S_v, \\ x &= X + S_h. \end{aligned} \qquad [1.8]$$

In these formulas, Y is the output variable, which stands for longitudinal force F_x or lateral force F_y or aligning moment M_z. X is the input variable, which stands for lateral slip angle α or longitudinal slip σ_x. Therefore, the following equations are deduced:

$$\begin{aligned} \overline{F_x}(\sigma_x + S_{hx}) &= D_x \sin[C_x \arctan(B_x\sigma_x - E_x(B_x\sigma_x - \arctan(B_x\sigma_x)))] + S_{vx}, \\ \overline{F_y}(\alpha + S_{hy}) &= D_y \sin[C_y \arctan(B_y\alpha - E_y(B_y\alpha - \arctan(B_y\alpha)))] + S_{vy}, \\ \overline{M_z}(\alpha + S_{hz}) &= D_z \sin[C_z \arctan(B_z\alpha - E_z(B_z\alpha - \arctan(B_z\alpha)))] + S_{vz}. \end{aligned} \qquad [1.9]$$

The parameters B, C, D, E, S_v and S_h of these formulas are defined as follows:

– D: the peak value.

– C: the shape factor that controls the limits of the range of the sine function appearing in formula [1.7] and thereby determines the shape of the resulting curve.

– B: the stiffness factor. This factor determines the slope at the origin and is also called the stiffness factor.

– E: the curvature factor; it controls the value of the slip at which the peak of the curve occurs.

– $B \times C \times D$: this product corresponds to the slope at the origin $(x = y = 0)$. For lateral force, this factor corresponds to the *cornering stiffness*.

In 1991, Pacejka proposed a model that takes into account the camber angle, the cornering stiffness and the load variations:

– for the longitudinal force parameters:

$$\begin{aligned} D_x &= F_z(b_1 F_z + b_2), \\ B_x &= \frac{1}{C_x D_x}(b_3 F_z + b_4) F_z \exp(-b_5 F_z), \\ C_x &= b_0, \\ E_x &= (b_6 F_z^2 + b_7 F_z + b_8)(1 - b_9 \text{sign}(g_l + S_{hx})), \\ S_{hx} &= b_{10} F_z + b_{11}, \\ S_{vx} &= b_{12} F_z + b_{13}; \end{aligned} \qquad [1.10]$$

– for the lateral force parameters:

$$\begin{aligned} D_y &= F_z(a_1 F_z + a_2)(1 - a_3 c^2), \\ B_y &= \frac{1}{C_y D_y} a_4 \text{sin}(2 \arctan(\frac{F_z}{a_5})(1 - a_6 \|c\|)), \\ C_y &= a_0, \\ E_y &= (a_7 F_z + a_8)(1 - (a_9 c + a_{10} \text{sign}(\beta_r + S_{hy}))), \\ S_{hy} &= a_{11} F_z + a_{12} + a_{13} c, \\ S_{vy} &= a_{14} F_z + a_{15} + c(a_{16} F_z^2 + a_{17} F_z); \end{aligned} \qquad [1.11]$$

– for the aligning torque parameters:

$$
\begin{aligned}
D_z &= F_z(c_1 F_z + c_2),\\
B_z &= -\frac{1}{C_z D_z} c_{12}\|c\|(c_3 F_z^2 + c_4 F_z)\exp(-c_5 F_z),\\
C_z &= c_0,\\
E_z &= -c_{12}\|c\|(c_6 F_z^2 + c_7 F_z + c_8),\\
S_{hz} &= c_9 c,\\
S_{vz} &= (c_{10} F_z^2 + c_{11} F_z)\|c\|.
\end{aligned}
\qquad [1.12]
$$

The variable c represents the camber angle. The parameters a_i, b_j and c_k are empirically identified. They depend on road structures and conditions (road friction, structure, etc.) and tire state (structure, pressure, shape, etc.).

To visualize the Magic formula, Figures 1.9, 1.10 and 1.11 show, respectively, the longitudinal, lateral and self-aligning moment evolutions for different vertical loads. When the wheel load increases, the tire can stick to the road better. We can easily distinguish the linear and nonlinear zone for these variables as discussed before. It will be noted that as the load increases, the peak of the longitudinal/lateral forces occurs at somewhat higher longitudinal slip ratio/slip angle. The slippage occurs at higher wheel slips. In the following, more discussion about tire forces, especially the lateral tire force, is presented.

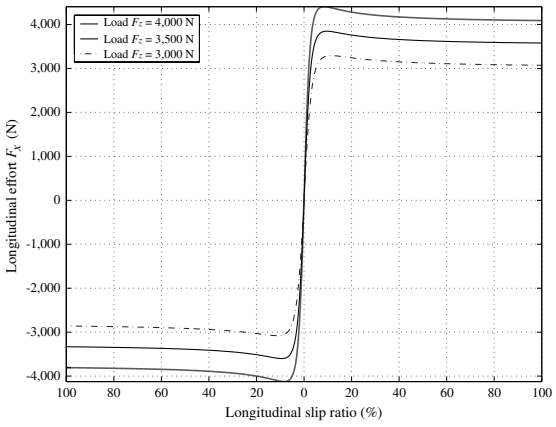

Figure 1.9. *Pacejka's model, longitudinal force versus slip ratio for different loads*

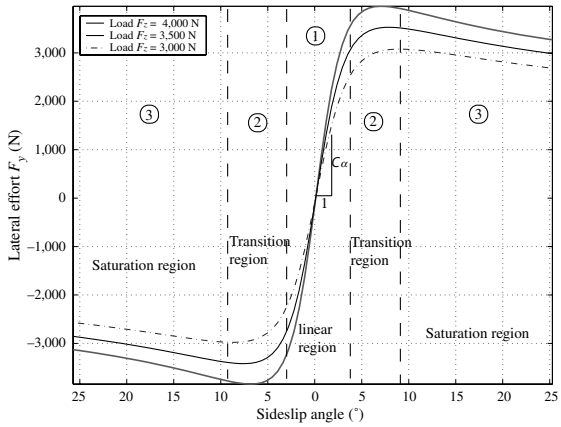

Figure 1.10. *Pacejka's model, lateral force versus sideslip angle for different loads*

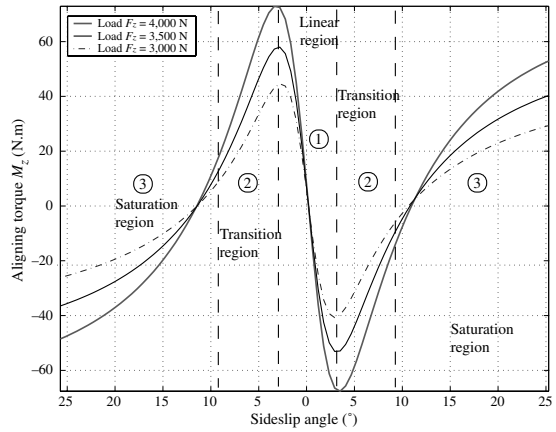

Figure 1.11. *Pacejka's model, auto-aligning torque versus sideslip angle for different loads*

Longitudinal force and longitudinal stiffness: from Figure 1.9, it is clear that in the case where the longitudinal slip is small (less than 0.1 on a dry surface), the longitudinal tire force is directly proportional to the slip ratio. The proportionality coefficient C_σ is called the longitudinal stiffness. It should be noted that the longitudinal slip ratio is typically small during normal (gentle) driving on a dry surface road. C_σ is a function of the tire load, road condition, and it is mainly determined by the tire construction.

Lateral force and cornering stiffness: for a constant load, the relationship between the side force and slip angle is initially linear, with a constant slope determined by the

cornering stiffness C_α (see Figure 1.10). This region of handling is called the linear operating region. As the slip angle grows, eventually the force starts to saturate due to limited friction on the road, entering the nonlinear region. Conceptually, cornering stiffness is a property of the tire (and to a lesser extent the road surface due to changes in the tire contact patch area), and changes slowly with time due to tire wear, inflation pressure and temperature fluctuations [SAK 82]. On the other hand, tire–road friction can change quickly; it depends on the road surface type (e.g. asphalt, gravel and dirt) and conditions (e.g. dry, wet and icy). Figure 1.12 shows how the cornering stiffness varies with load changes according to Pacejka's formula. A closer investigation reveals that the nonlinear region of the lateral force can be decomposed into transition and saturation regions. In the transition region, lateral force increases with the sideslip angle, but in proportion less than the linear case. The tire slips in the saturation zone. The nonlinear zone represents the tire limits and it is rarely reached under normal driving conditions. If the front tires saturate first, the vehicle is said to display understeer, and may plow out of a bend. If the rear tires saturate first, the vehicle limits oversteers and may spin out. Because most drivers are not accustomed to operating in the nonlinear handling regime, both of these responses are potentially very dangerous, even if understeer is much easier to cope with for most drivers than oversteer.

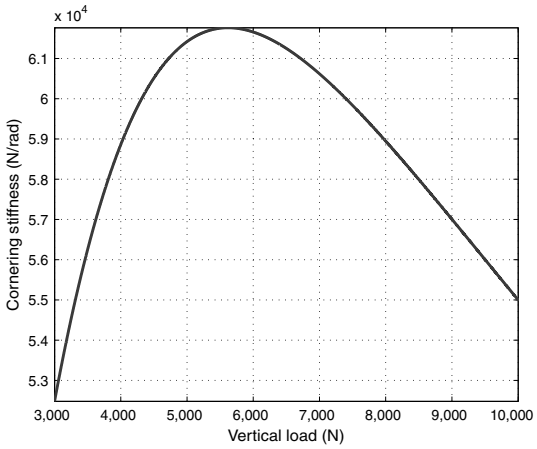

Figure 1.12. *Pacejka's model, cornering stiffness versus vertical loads*

Auto-aligning moment: the self-auto-aligning moment decreases in the transition zone until it changes sign in the saturation zone. Finally, it converges to zero for high sideslip angles. This is not the case in Figure 1.11. Pacejka's model defect is discussed by different authors, as in [MIL 95] and [JAZ 08], and hence is not considered in detail here.

Effect of camber angles: among factors other than the load, the camber angle also plays an important role on the behavior of the vehicle. The camber angle is defined as the inclination of the wheel from its vertical position (see Figure 1.13). Or, more precisely, camber is the inclination from a plane perpendicular to the ground. It is positive if the wheel leans outward at the top relative to the vehicle, or negative if it leans inward. A non-zero camber angle produces a camber force creating another component of lateral force. Thus, a negative camber angle increases the lateral force of the tire. Camber's effect on lateral force and aligning torque is shown in Figure 1.14.

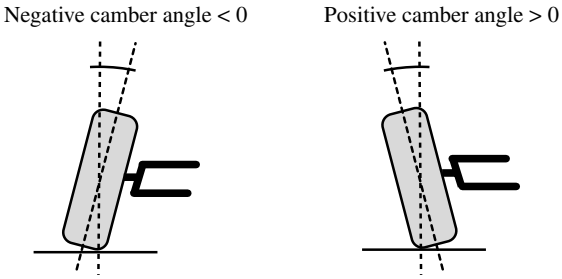

Figure 1.13. *Camber angle*

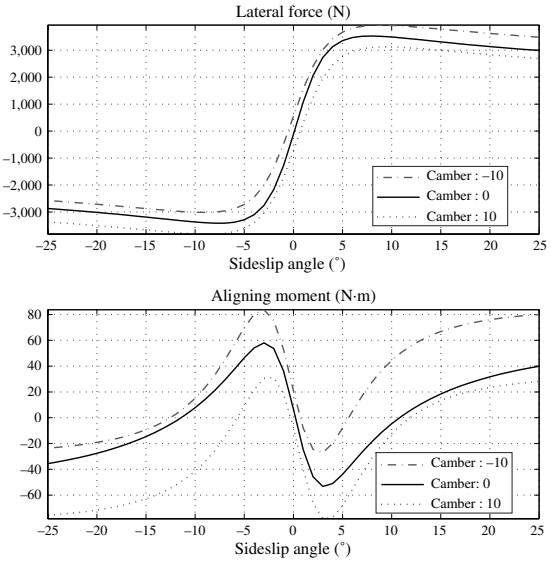

Figure 1.14. *Pacejka's model, influence of camber angle on lateral force and on auto-alignment*

Comparing the lateral force produced by the camber angle to that produced by a slip angle, it is obvious that the latter is more significant. Although the camber force is usually less than the lateral force due to the slip angle, the camber force can have a significant impact on vehicle handling, especially as the suspension geometry changes. The effect of camber force will be neglected in the following chapters for reasons of simplicity. Thus, the lateral force is assumed to be generated only by slip angles.

In addition to the problems caused by the need to identify these model parameters, the combined aspect between longitudinal and lateral phenomena does not appear in this current version of Pacejka's model. This means that this model does not show the effect of the sideslip angle on the longitudinal forces and the effect of longitudinal slip on lateral forces and the aligning moment. To take into account these coupling effects, more parameters are needed [PAC 02]. For reasons of simplicity, this coupling model will not be used in the following chapters, and therefore is not presented here. In this topic, readers could also refer to [BAY 93] where a purely empirical method is discussed using Magic formula-based functions to describe the tire force generation at combined slip.

1.2.3.2. *Dugoff's tire model*

Dugoff's tire model presented in the following is the simplification version of the HRSI model [DUG 69, DUG 70]. It provides a simple formulation and the ability to describe forces under pure cornering, pure acceleration/braking and combined acceleration(braking)/cornering maneuvers. It assumes a uniform vertical pressure distribution on the tire contact patch. Compared to the Magic formula tire model, Dugoff's model offers one significant advantage; it synthesizes all the tire property parameters into two constants, C_σ and C_α, called longitudinal and cornering (lateral) stiffness of the tire. Let σ_x, defined in equation [1.1], be the longitudinal slip ratio of the tire under consideration and α be the slip angle. Then, the longitudinal tire force is given by:

$$\overline{F_x} = -C_\sigma \frac{\sigma_x}{1+\sigma_x} f(\lambda), \qquad [1.13]$$

and the lateral tire force is given by:

$$\overline{F_y} = -C_\alpha \frac{\tan\alpha}{1+\sigma_x} f(\lambda), \qquad [1.14]$$

where $f(\lambda)$ is given by:

$$f(\lambda) = \begin{cases} (2-\lambda)\lambda, & \text{if } \lambda < 1 \\ 1, & \text{if } \lambda \geq 1 \end{cases} \qquad [1.15]$$

$$\lambda = \frac{\mu F_z (1+\sigma_x)}{2\left\{(C_\sigma \sigma_x)^2 + (C_\alpha \tan\alpha)^2\right\}^{1/2}}. \qquad [1.16]$$

It is obvious that both formulas are functions of four fundamental physical tire properties: the tire's slip and stiffness, normal force and tire–road friction coefficient. Note that the tire self-aligning torque description is absent in this model.

Dugoff's tire model considers a coupled relationship between longitudinal and lateral tire forces. This is due to the fact that there is a limited amount of tire force that can be generated in the contact patch. The tire adhesion capability used for generating longitudinal tire force therefore limits how much lateral tire force can be generated in the contact patch, and vice versa. This coupled relationship is often called the *friction circle* or the *friction ellipse* concept. For further information concerning this concept, the reader can refer to [PAC 02].

1.2.3.3. *Linear model*

Under normal driving conditions (lateral acceleration below 0.4 g), the tires are well away from saturation and have small slip and slip angle values. Under these types of conditions, the longitudinal and lateral forces are approximately linear functions of the slip and slip angle with a slope equal to the cornering stiffness. As a result, it is common to use this linear approximation for the tire forces:

$$\begin{aligned} \overline{F_x}(\sigma_x) &= -C_\sigma \sigma_x, \\ \overline{F_y}(\alpha) &= -C_\alpha \alpha. \end{aligned} \qquad [1.17]$$

As mentioned earlier, the longitudinal and cornering stiffness C_x and C_y, respectively, depend essentially on the road friction and on the tire load and construction.

When using these linear approximations, it is important to understand the operating region of the tires for the specific application. Typically, the linear tire model predicts real tire behavior for vehicle acceleration under 0.4 g [GIL 92, MIL 95, RAJ 06, JAZ 08] (normal driving conditions). Tires are very nonlinear beyond 0.4 g and eventually saturate with subsequent degradation in force capability (i.e. see Figure 1.10). Owing to the negligence of the effort saturation, the tire forces tend to be overestimated by the linear model, especially when the tire slip is significant. The potential of limitation of linear models has been studied in detail in [LEC 02].

1.2.4. *Transient tire model*

The dynamic behavior of the tire has lately gained a wide interest. In general, tire forces are not developed instantaneously at maneuvering actions, but require a certain rolling distance of the tire to build up due to the flexible structure. This means that the force and associated moment response of a tire to various external inputs is delayed. Such inputs include the vertical load, the steer angle and the camber angle. This delayed response manifests itself in the dynamic (or transient) tire behavior [LOE 90].

A typical dynamic model that can be used for lateral tire force dynamics is of first order and presented by [BOL 99, RAJ 06]:

$$\tau \dot{F}_y + F_y = \overline{F_y}, \quad [1.18]$$

where τ is the relaxation time constant, F_y the dynamic lateral force and $\overline{F_y}$ the lateral tire force calculated from a quasi-static reference tire model.

τ can be approximated by:

$$\tau = \frac{C_\alpha}{K V_x}, \quad [1.19]$$

where V_x is the vehicle longitudinal velocity, C_α the cornering stiffness and K the equivalent tire lateral stiffness. Multiplying the relaxation time constant by the vehicle speed gives the relaxation length:

$$\sigma = \frac{C_\alpha}{K}, \quad [1.20]$$

where σ is the approximate distance needed to build up tire forces.

Equation [1.18] can be rewritten as follows:

$$\dot{F}_y = \frac{V_x}{\sigma}(-F_y + \overline{F_y}). \quad [1.21]$$

Owing to the presence of longitudinal velocity in the denominator in equation [1.19], this model is not valid for low velocities [RAJ 06]. It has also been shown that experimentally measured lateral tire forces have under-damped characteristics at high speed. Changing the tire dynamic model from first-order lateral tire force dynamics to second-order slip angle dynamics helps capture the under-damped tire dynamics accurately.

1.3. Wheel rotational dynamics

Now, let us focus on the wheel rotational dynamics. The model represented in Figure 1.15 is usually used when studying longitudinal dynamics. For each of the wheels ij, a separate equation of motion must be derived, relating the angular acceleration $\dot{w}_{ij}$ to the transmitted wheel torque T_{ij} and longitudinal tire force F_{xij}. The equation for a wheel is typically:

$$T_{ij} - R_{\mathrm{eff}_{ij}} F_{xij} = I_{wij} \dot{w}_{ij}, \quad [1.22]$$

where I_{wij} is the moment of inertia of the wheel, $\dot{w}_{ij}$ its angular velocity and $R_{\mathrm{eff}_{ij}}$ the effective tire radius.

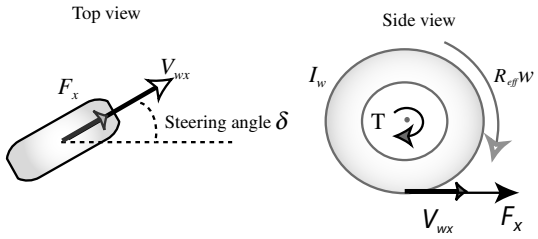

Figure 1.15. *Wheel longitudinal dynamic model*

Note that the tire roughly behaves like a spring in response to the vertical force applied to it. Therefore, its radius R_{eff} is not constant and it varies during the vehicle movement as a function of the load and of the angular wheel velocity. The following sections provide analysis and formulations concerning the tire radius.

1.3.1. *Static tire radius*

The static tire radius R_{stat} relates the stationary wheel ground contact force F_z to the tire vertical spring stiffness k_t [KIE 00], as shown in Figure 1.16:

$$R_{\text{stat}} = R_0 - \frac{F_z}{k_t}, \qquad [1.23]$$

where R_0 is the undeformed radius of the tire and F_z/k_t is the tire vertical deflection.

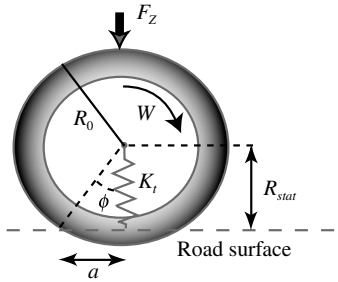

Figure 1.16. *Static and dynamic wheel radius (figure deduced from [KIE 00])*

1.3.2. *Effective tire radius*

The effective tire radius R_{eff} is the value of the radius that relates the rotational angular velocity of the wheel, w, to the linear longitudinal velocity of the wheel, V_{wx}, as it moves through the contact patch of the tire with the ground.

If the rotational speed of the wheel is w, the linear equivalent of the rotational speed of the tire is $V_{wx} = R_{\text{eff}} w$ [KIE 00].

As shown in Figure 1.16, let $2a$ be the longitudinal length of the contact patch and ϕ be the angle made by the radial line joining the center of the wheel to the end of the contact patch. Let t be the duration of time taken by an element of the tire to move through half the contact patch. According to [RAJ 06]:

$$V_{wx} = R_{\text{eff}} w = \frac{a}{t}. \quad [1.24]$$

At the same time, the rotational speed of the wheel is:

$$w = \frac{\phi}{t}. \quad [1.25]$$

Hence

$$R_{\text{eff}} = \frac{a}{\phi}. \quad [1.26]$$

From the geometric relationships seen in Figure 1.16:

$$R_{\text{stat}} = R_0 \cos\phi, \quad [1.27]$$

$$a = R_{\text{stat}} \sin\phi. \quad [1.28]$$

Therefore, the effective tire radius is given by:

$$R_{\text{eff}} = \frac{\sin\left[\arccos\left(\frac{R_{\text{stat}}}{R_0}\right)\right]}{\arccos\left(\frac{R_{\text{stat}}}{R_0}\right)}. \quad [1.29]$$

Note that $R_{\text{eff}} = \sin\phi/\phi R_0$, $R_{\text{eff}} < R_0$, and that since $R_{\text{eff}} = \tan\phi/\phi R_{\text{stat}}$, $R_{\text{eff}} > R_{\text{stat}}$. Thus, $R_{\text{stat}} < R_{\text{eff}} < R_0$.

The variations to the vertical load, the tire pressure and temperature make R_{eff} calculation a difficult task. This difficulty also affects the longitudinal slip calculation (see section 1.2.1.2).

1.4. Vehicle body dynamics

After presenting the basic tire properties in the previous sections, it is relatively straightforward to develop vehicle models that capture the important dynamics of the vehicle.

The vehicle system can be divided into two parts: sprung part mass and unsprung part mass. The sprung part includes all the components supported by the suspensions

such as the vehicle body, internal components, passengers and cargo, but not the mass of the suspension components themselves. The unsprung part includes the suspensions, wheels and other components directly connected to them. For passenger cars and commercial vehicles, the majority of the vehicle mass is sprung. The larger the ratio of sprung mass to unsprung mass, the less the body and vehicle occupants are affected by road bumps, dips and other surface imperfections. The vehicle sprung mass can be lumped as a rigid body. Its motions comprise X, Y and Z motions, as well as yaw, roll and pitch motions, as shown in Figure 1.17.

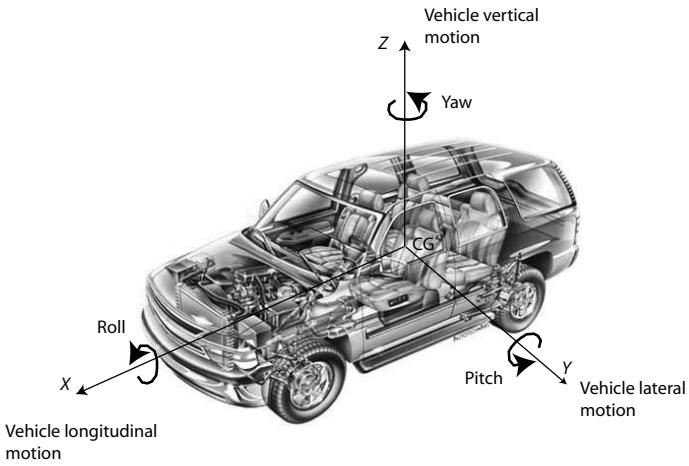

Figure 1.17. *Vehicle body motions*

In this section, vehicle dynamics are presented with the emphasis on simplified vehicle dynamic models. The objective is to use these models as basic elements when building real-time estimators in the subsequent chapters. In the following, we present notably:

– the suspension dynamics through a quarter-car model;

– the four-wheel and bicycle vehicle models that describe the planar motion of a vehicle behavior;

– the roll model that introduces the roll behavior, taking into account the suspension kinematics.

1.4.1. *Vehicle's vertical dynamics*

Driving on an uneven road surface, the vehicle body moves upward and downward. The following sections are devoted to understanding the vertical motion of the vehicle, using suspension models. In the literature, full-, half- and quarter-car suspension

models can be found. In this section, and after describing the main suspension roles, only the quarter-car model will be presented. For further information on suspension dynamics, the reader can refer to [MIL 95], [BAS 04] and [RAJ 06].

1.4.1.1. *Suspension functions*

According to [BAS 04], the automotive suspension on a vehicle typically has the following basic tasks:

Isolating a car body from road disturbances to provide good ride quality: ride quality in general can be quantified by the vertical acceleration of the passenger locations. The presence of a well-designed suspension provides isolation by reducing the vibratory forces transmitted from the axle to the vehicle body. This in turn reduces vehicle body acceleration. In the case of the quarter-car suspension (see Figure 1.18), sprung mass acceleration $\ddot{z}_s$ can be used to quantify ride quality.

Keeping good road holding: the road holding performance of a vehicle can be characterized in terms of its cornering, braking and traction abilities. Improved cornering, braking and traction are obtained if the variations in normal tire loads are minimized. This is because the lateral and longitudinal forces generated by a tire depend directly on the normal tire load. Since the tire radius depends on vertical forces, variations in tire load can be directly related to vertical tire deflection (i.e. $(z_u - u)$ in Figure 1.18). The road holding performance of a suspension can therefore be quantified in terms of the tire deflection performance.

Providing good handling: the roll and pitch accelerations of a vehicle during cornering, braking and traction are measures of good handling. A good suspension system should ensure that roll and pitch motions are minimized.

Supporting the vehicle's static weight: this task is performed well if the rattle space requirements in the vehicle are kept small. In the case of the quarter-car model, it can be quantified in terms of the maximum suspension deflection (i.e. $(z_s - z_u)$ in Figure 1.18) undergone by the suspension.

1.4.1.2. *Quarter-car vehicle model*

The most commonly used and useful model of a vehicle suspension system is a two degree-of-freedom (2DOF) quater-car model, as shown in Figure 1.18. It represents the vertical vibration of a vehicle and is usually used to describe the vertical dynamics of a vehicle that runs at a constant speed along an uneven road. This model is made up of two solid masses m_{qs} and m_{qu} denoted as quarter sprung and unsprung masses, respectively. The quarter sprung mass represents one-fourth of the body of the vehicle and the quarter unsprung mass m_{qu} represents one wheel of the vehicle. A spring of stiffness k_s and a shock absorber with viscous damping coefficient c_s support the sprung mass and are called the main suspension. The unsprung mass m_{qu} is in direct

contact with the ground through a spring k_u and damper coefficient c_u, representing, respectively, the tire stiffness and the tire damper. z_s is the position of the vehicle body, z_u the position of the wheel and u the displacement of the road. This model does not take into account pitch and roll motions.

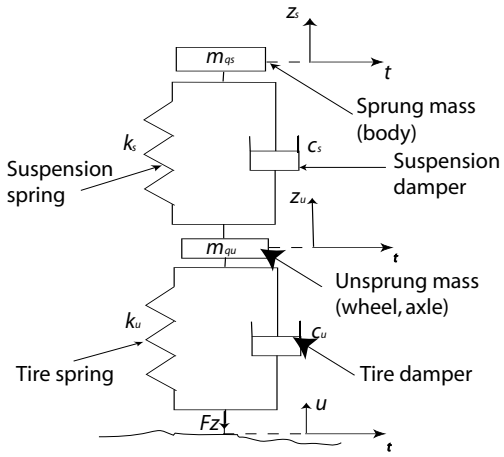

Figure 1.18. *Quarter-car model*

Despite its simplicity, this model captures the most basic feature of the vertical model of the vehicle. It is widely used when designing suspension [LOY 09], developing suspension control algorithms [ELM 99, GEO 07, SAV 10] and studying road profile [DOU 11b].

Assuming the wheels are rolling without slip and without contact loss, the vehicle body and the wheel motions can be given by relations [1.30] and [1.31], respectively:

$$m_{qs}\ddot{z}_s = -k_s z_s - c_s\dot{z}_s + k_s z_u + c_s\dot{z_u}, \quad [1.30]$$

$$m_{qu}\ddot{z}_u = -(k_s + k_u)z_u - (c_s + c_u)\dot{z}_u + k_s z_s + c_s\dot{z}_s + k_u u + c_u\dot{u}. \quad [1.31]$$

Taking into account the suspension dynamics, the vertical force F_z on a wheel can be calculated according to the following formulas:

$$F_z = (m_{qs} + m_{qu})g - k_u(z_u - u) - c_u(\dot{z_u} - \dot{u}) \quad [1.32]$$

or

$$F_z = m_{qu}\ddot{z}_u - k_s(z_s - z_u) - c_s(\dot{z}_s - \dot{z_u}), \quad [1.33]$$

where g is the gravitational acceleration.

1.4.2. *Vehicle planar dynamics*

In this section, dynamic models for a rigid vehicle in a planar motion are developed. When the forward, lateral and yaw velocities are significant and somehow enough to examine the behavior of a vehicle, the planar models are applicable. Thereby, a lot of publications can be found in the literature that deal with the modeling of the vehicle in a plane [KIE 00, RAJ 06, JAZ 08].

In the following, the *four-wheel vehicle model* (FWVM) is presented, leading to a more simplified *bicycle model*. Keeping in mind that the main goal of this chapter is to describe in real time the vehicle dynamics with an acceptable computational cost, these models will be simplified in a reasonable manner.

1.4.2.1. *Four-wheel vehicle model*

The FWVM, commonly called the two tracks model, is widely used in the literature to study and control the longitudinal and transversal vehicle dynamic behavior [RAY 97, WEN 06, OSB 06]. This model has the advantage that it clearly represents the four wheels. Figure 1.19 shows the schematic of a 3DOF vehicle model that represents the longitudinal, lateral and yaw motions. This model ignores heave, roll and pitch motions and has no suspension. The front and rear track widths E are assumed to be equal. The distances from the vehicle's center of gravity (COG) to the front and rear axles are l_f and l_r, respectively. Assuming rear steering angles are approximately null, the direction or heading of the rear tires is the same as that of the vehicle. The heading of the front tires includes the steering angle (δ). The front steering angles are assumed to be equal ($\delta_{11} = \delta_{12} = \delta$).

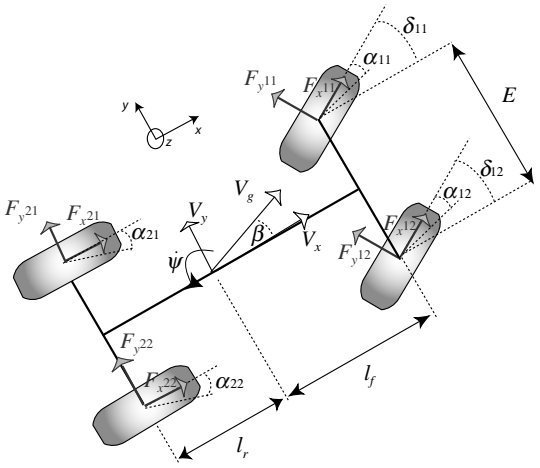

Figure 1.19. *2D schema representation of a four-wheel vehicle model*

The sideslip at the vehicle's center of gravity (β) is the angle between the velocity vector (V_g) and the true heading of the vehicle (ψ) . The yaw rate ($\dot{\psi}$) is the angular velocity of the vehicle about the vertical axis, with I_z being the yaw moment of inertia. The longitudinal and lateral velocities are V_x and V_y, respectively. The longitudinal and lateral forces ($F_{x,y,i,j}$), acting during the movement, are shown for front and rear tires of the vehicle.

The inter-relationship between the different vehicle dynamic parameters can be described by differential equations. Applying Newton's second law to the lumped vehicle mass longitudinally, laterally and about a vertical axis through the center of mass produces the following equations of motion [KIE 00, SHR 07]:

$$\ddot{\psi} = \frac{1}{I_z}\begin{bmatrix} l_f[F_{y11}\cos\delta + F_{y12}\cos\delta + F_{x11}\sin\delta + F_{x12}\sin\delta] \\ -l_r[F_{y21} + F_{y22}] + \frac{E}{2}[F_{y11}\sin\delta - F_{y12}\sin\delta \\ +Fx_{12}\cos\delta - Fx_{11}\cos\delta + F_{x22} - F_{x21}] \end{bmatrix}, \quad [1.34]$$

$$\dot{\beta} = -\dot{\psi} + \frac{1}{m_v V_g}\begin{bmatrix} -(F_{x11} + Fx_{x12})\sin(\beta-\delta) \\ +F_{y11}\cos(\beta-\delta) + F_{y12}\cos(\beta-\delta) \\ +F_{y11}\cos(\beta-\delta) + (F_{y21} + F_{y22})\cos\beta \\ -(F_{x21} + Fx_{22})\sin\beta \end{bmatrix}, \quad [1.35]$$

$$a_y = \frac{1}{m_v}\begin{bmatrix} F_{y11}\cos\delta + F_{y12}\cos\delta + (F_{y21} + F_{y22}) \\ +F_{x11}\sin\delta + F_{x12}\sin\delta \end{bmatrix}, \quad [1.36]$$

$$a_x = \frac{1}{m_v}\begin{bmatrix} -F_{y11}\sin\delta - F_{y12}\sin\delta + F_{x11}\cos\delta + F_{x12}\cos\delta \\ +F_{x21} + F_{x22} \end{bmatrix}, \quad [1.37]$$

$$\dot{V_x} = V_y\dot{\psi} + a_x, \quad [1.38]$$

$$\dot{V_y} = -V_x\dot{\psi} + a_y, \quad [1.39]$$

$$\dot{V_g} = \frac{1}{m_v}\begin{bmatrix} (F_{x11} + F_{x12})\cos(\beta-\delta) + F_{y11}\sin(\beta-\delta) \\ +F_{y12}\sin(\beta-\delta) + (F_{x21} + F_{x22})\cos\beta + \\ (F_{x21} + F_{x22})\cos\beta + (F_{y21} \\ +F_{y22})\sin\beta \end{bmatrix}. \quad [1.40]$$

Using integrals of the vehicle's longitudinal, lateral and yaw accelerations, the velocity of each wheel hub in the rolling direction of that wheel can be derived [OSB 06]:

$$V_{wx11} = \left(V_x - \frac{\dot{\psi}E}{2}\right)\cos\delta + (V_y + \dot{\psi}l_f)\sin\delta, \quad [1.41]$$

$$V_{wx12} = \left(V_x + \frac{\dot{\psi} E}{2} \right) \cos\delta + (V_y + \dot{\psi} l_f) \sin\delta, \quad [1.42]$$

$$V_{wx21} = V_x - \frac{\dot{\psi} E}{2}, \quad [1.43]$$

$$V_{wx22} = V_x + \frac{\dot{\psi} E}{2}. \quad [1.44]$$

The longitudinal and lateral velocities, the steer angle of the front wheels and the yaw rate are then used as a basis for the calculation of the tire slip angles α_{ij} as well as the vehicle body slip angle β:

$$\alpha_{11} = \delta - \arctan\left[\frac{V_y + l_f \dot{\psi}}{V_x - E\dot{\psi}/2} \right], \quad [1.45]$$

$$\alpha_{12} = \delta - \arctan\left[\frac{V_y + l_f \dot{\psi}}{V_x + E\dot{\psi}/2} \right], \quad [1.46]$$

$$\alpha_{21} = -\arctan\left[\frac{V_y - l_r \dot{\psi}}{V_x - E\dot{\psi}/2} \right], \quad [1.47]$$

$$\alpha_{22} = -\arctan\left[\frac{V_y - l_r \dot{\psi}}{V_x + E\dot{\psi}/2} \right], \quad [1.48]$$

$$\beta = \arctan\frac{V_y}{V_x}. \quad [1.49]$$

1.4.2.2. *Wheel-ground vertical forces calculation*

In moderate driving situations, the vertical forces are mainly caused by the Earth's gravity. These forces primarily depend on the passenger and package distribution, and on the geometric features of the vehicle. During acceleration, braking or cornering, the vehicle body shifts because of inertial forces. First, the individual vertical wheel forces change depending on the accelerations acting on the spring damper characteristics of the suspension system and on kinematic interactions of the coupled wheels. Considering all of these effects results in a set of complex nonlinear equations with many unknown parameters that have to be identified. To avoid complexity, the vertical wheel forces are approximated with a simple approach here. The camber angle is neglected as well as the suspension dynamics. The roll and pitch accelerations $\ddot{\theta}$ and $\ddot{\varphi}$ are not considered. Furthermore, the roll and pitch axes are assumed to pass through the COG.

The current wheel loads depend on the longitudinal and lateral accelerations. Positive longitudinal acceleration a_x causes a pitch motion of the vehicle body due

to its inertia. The pitch motion relieves the front axle and loads the rear axle (see Figure 1.20). This model is based on the study presented in [KIE 00].

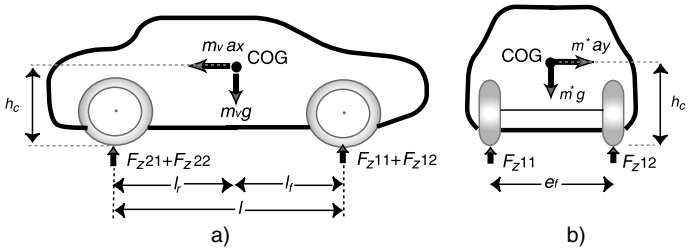

Figure 1.20. *(a) Wheel load changes for positive longitudinal accelerations and (b) wheel load changes on the front axle for lateral accelerations in a left curve*

The torque balance about the wheel ground contact point of the rear axle provides:

$$lFz_1 = l_r m_v g - m_v h_c a_x, \qquad [1.50]$$

where Fz_1 is the vertical load on the front tires and m_v the vehicle mass. Consequently:

$$Fz_1 = m_v \left(\frac{l_r}{l} g - \frac{h_c}{l} a_x \right). \qquad [1.51]$$

Here, it is assumed that not only the vehicle body but also the whole vehicle rotates around the front wheel contact point. This is the reason for equation [1.51] containing the complete vehicle mass m_v instead of the vehicle body mass.

Second, during cornering, the lateral acceleration causes a roll torque that increases the load on the outside and decreases it on the inside of the vehicle.

The two axles are considered to be decoupled from one another. In the case of the front axle load, a virtual mass m^* is used:

$$m^* = \frac{Fz_1}{g} = \frac{m_v \left(\frac{l_r}{l} g - \frac{h_c}{l} a_x \right)}{g}. \qquad [1.52]$$

This virtual mass takes into account the mass transfer during acceleration. Consequently, this mass will be used as a coupling term between longitudinal and lateral dynamics.

Supposing the COG is located in the middle of the vehicle's lateral axis, the torque balance equation at the ground contact point of the front left wheel gives:

$$Fz_{12} e_f = m^* g \frac{e_f}{2} + m^* a_y h_c. \qquad [1.53]$$

Substituting the virtual mass m^* of equation [1.52] and solving for Fz_{12} gives the front right dynamic wheel force. By analogy for the other wheel vertical forces, these can be formulated as follows:

$$Fz_{11} = \frac{1}{2}m_v\left(\frac{l_r}{l}g - \frac{h_c}{l}a_x\right) - m_v\left(\frac{l_r}{l}g - \frac{h_c}{l}a_x\right)\frac{h_c}{e_f g}a_y, \quad [1.54]$$

$$Fz_{12} = \frac{1}{2}m_v\left(\frac{l_r}{l}g - \frac{h_c}{l}a_x\right) + m_v\left(\frac{l_r}{l}g - \frac{h_c}{l}a_x\right)\frac{h_c}{e_f g}a_y, \quad [1.55]$$

$$Fz_{21} = \frac{1}{2}m_v\left(\frac{l_f}{l}g + \frac{h_c}{l}a_x\right) - m_v\left(\frac{l_f}{l}g + \frac{h_c}{l}a_x\right)\frac{h_c}{e_r g}a_y, \quad [1.56]$$

$$Fz_{22} = \frac{1}{2}m_v\left(\frac{l_f}{l}g + \frac{h_c}{l}a_x\right) + m_v\left(\frac{l_f}{l}g + \frac{h_c}{l}a_x\right)\frac{h_c}{e_r g}a_y. \quad [1.57]$$

If couplings between the pitch and roll dynamics are not regarded ($m^* = m_v l_r/l$), the torque balances around the respective axes can be carried out separately. Therefore, the model becomes linear and vertical forces can be given by:

$$Fz_{11} = m_v g\frac{l_r}{2l} - m_v\frac{h_c}{2l}a_x - m_v\frac{h_c l_r}{e_f l}a_y, \quad [1.58]$$

$$Fz_{12} = m_v g\frac{l_r}{2l} - m_v\frac{h_c}{2l}a_x + m_v\frac{h_c l_r}{e_f l}a_y, \quad [1.59]$$

$$Fz_{21} = m_v g\frac{l_f}{2l} + m_v\frac{h_c}{2l}a_x - m_v\frac{h_c l_f}{e_r l}a_y, \quad [1.60]$$

$$Fz_{22} = m_v g\frac{l_f}{2l} + m_v\frac{h_c}{2l}a_x + m_v\frac{h_c l_f}{e_r l}a_y. \quad [1.61]$$

This assumption of linearity implies the validity of the superposition principle [MIL 95, LEC 02]. This principle states that the sum of a series of effects considered concurrently is identical to the sum of the individual effects considered individually. Therefore, the changes in wheel loads resulting from lateral and longitudinal load transfer could be numerically added to produce loads that are valid for combined operational conditions.

Without a suspension between the body and wheels, these models cannot predict the transient load shift effect during the acceleration, braking and cornering. The above normal force calculation methods are based on static force models and ignore the influence of the vibrations of the suspension. These methods give a reasonable estimate of the normal force, when the road surface is fairly well paved and not bumpy. However, if the road surface is very bumpy, a dynamic normal force estimation method incorporating the suspension dynamics will provide a more accurate calculation of the normal forces.

1.4.2.3. *Bicycle model*

The modeling of the vehicle movement can be considerably simplified by using a simplified bicycle model of the vehicle as shown in Figure 1.21. It is also known as the *single track model*. This model was developed by Segel in 1956 [SEG 56] and is currently used to describe the lateral vehicle-dynamic behavior, especially when evaluating sideslip angles [STE 07] and studying efforts per axle [BAF 08]. It can be seen as a simplification of the FWVM. The two left and right front wheels are represented by one single wheel. Similarly, the rear wheels are represented by one central rear wheel. In this model, vertical movements are ignored, roll motion is not taken into account, rear steering angles are null and front steering angles are assumed equal. The simplified bicycle model is formulated by the following relationship:

$$\ddot{\psi} = \frac{1}{I_z}\left[\ l_f[F_{x1}\sin\delta + F_{y1}\cos\delta] - l_r F_{y2}\ \right], \qquad [1.62]$$

$$\dot{\beta} = \frac{1}{m_v V_g}\left[\begin{array}{l} -F_{x1}\sin(\beta-\delta) + F_{y1}\cos(\beta-\delta) + \\ F_{y2}\cos\beta - F_{x2}\sin\beta \end{array}\right] - \dot{\psi}, \qquad [1.63]$$

$$\dot{V_g} = \frac{1}{m_v}\left[\begin{array}{l} F_{x1}\cos(\delta-\beta) - F_{y1}\sin(\delta-\beta) + F_{x2}\cos\beta + \\ F_{y2}\sin\beta \end{array}\right]. \qquad [1.64]$$

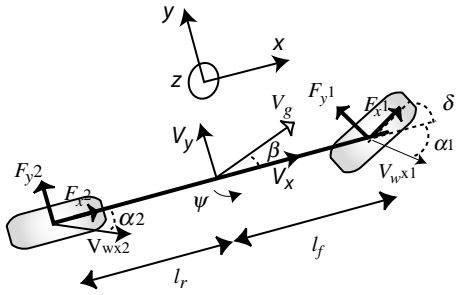

Figure 1.21. *Bicycle model*

Assuming small angles, front and rear tire sideslip angles are calculated using kinematic relations with respect to the vehicle's speed and yaw rate [RAJ 06]:

$$\alpha_1 = \delta - \beta - l_f\frac{\dot{\psi}}{V_x}, \qquad [1.65]$$

$$\alpha_2 = -\beta + l_r\frac{\dot{\psi}}{V_x}. \qquad [1.66]$$

The lateral ($F_{yi} = F_{yi1} + F_{yi2}$) and vertical ($F_{zi} = F_{zi1} + F_{zi2}$) forces acting on front and rear tires (*per front and rear axles*) can be written as:

$$F_{y1} = \frac{m_v a_y l_r - I_z \ddot{\psi}}{(l_f + l_r)\cos\delta}, \quad [1.67]$$

$$F_{y2} = \frac{m_v a_y l_f + I_z \ddot{\psi}}{(l_f + l_r)}, \quad [1.68]$$

$$F_{z1} = \frac{m_v (g l_f - a_x h_c)}{l_f + l_r}, \quad [1.69]$$

$$F_{z2} = \frac{m_v (g l_r + a_x h_c)}{l_f + l_r}, \quad [1.70]$$

where $\ddot{\psi}$ is the yaw angular acceleration.

Compared to the bicycle model, the FWVM can provide a much more accurate vehicle description, particularly of the lateral dynamics. Regarding all four wheels, the FWVM allows us to consider load changes. It is obvious that when using a bicycle model, the differences in the left and right tires cannot be considered in its formulation. However, as we have seen in section 1.4.2.2, the vertical forces of the right and left tires on both front and rear axles could be different due to the vehicle roll moment.

1.4.3. *Roll dynamics and lateral load transfer evaluation*

Rotational motion of a vehicle is composed of yaw, roll and pitch motions. While yaw motion is indispensable for turning, roll and pitch motions are derived from the suspension mechanism. These motions affect important characteristics of vehicle dynamics and deserve to be considered. In the following, some important features of the vehicle roll behavior are described.

Usually in the literature, two vehicle models are used in order to describe the roll motion:

– Yaw-roll 3DOF model, which represents yaw, lateral and roll motions of a vehicle [RYU 06];

– 1DOF model, which represents only the roll motion of a vehicle. It is also called the roll plane model (see Figure 1.22). Although simple, this model provides robust results [RYU 06].

The roll plane is usually used when studying the lateral load transfer due to the roll motion [ALE 04]. It is also used when defining some rollover index parameters [ALE 02, YOO 07]. During handling maneuvers on smooth roads, vehicle roll motion

is primarily induced by centrifugal forces caused by lateral accelerations. In this case, the roll motion of the vehicle body can be presented by a roll model including the roll angle θ, as shown in Figure 1.22. This semi-car model has a roll DOF for the suspension that connects the sprung and unsprung masses.

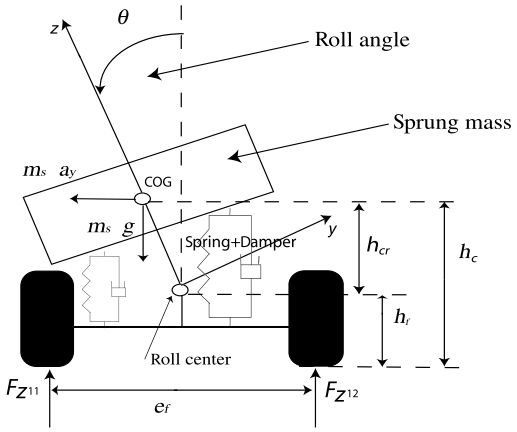

Figure 1.22. *Roll plane model*

In this model, during cornering, the sprung mass is assumed to rotate about the roll axis. The roll axis is defined as the line that passes through the roll center at the front and rear axles (see Figure 1.23). It is determined by the mechanism of suspensions [OZA 02]. The roll center is the point in the transverse vertical plane through any pair of wheel centers and equidistant from them, at which lateral forces may be applied to the sprung mass without producing a roll angle displacement of the sprung mass [MIL 95]. The front and rear roll centers can be constructed from the lateral motion of the wheel contact points. In reality, the roll centers of the vehicle do not remain constant, but in the following, stationary roll centers are assumed to simplify the model. The suspension system is modeled as a linear spring-damper system. The roll angle depends on the roll stiffness of the axle and on the positions of the roll centers.

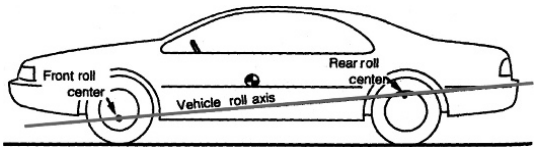

Figure 1.23. *Roll centers and roll axis (figure deduced from [GIL 92])*

The body roll motion with respect to the road is caused by the inertial force due to lateral acceleration, $m_s a_y$, which produces the moment $m_s a_y h_{cr}$ about the roll axis.

For a significant roll angle, a component of gravity force, $m_s g \sin\theta$, also contributes to the roll moment.

According to the torque balance in the roll axis, the roll dynamics of the vehicle body can be described by the following differential equation [DIN 05]:

$$I_{xx}\ddot{\theta} + C_R\dot{\theta} + K_R\theta = m_s a_y h_{cr} + m_s h_{cr} g \sin\theta, \quad [1.71]$$

where I_{xx} is the moment of inertia of the sprung mass m_s with respect to the roll axis, C_R and K_R, respectively, the total damping and spring coefficients of the roll motion of the vehicle system (combined roll dynamics of suspensions and tires), h_{cr} the height of the sprung mass about the roll axis and g the gravitational constant. Note that the model does not take into account the excitation due to road unevenness.

The roll angle, θ, can be found by integrating equation [1.71]. However, during most steady-state handling maneuvers, the first two terms can be neglected. Assuming a small roll angle, this yields the simplified roll angle is estimated as:

$$\theta = \frac{m_s a_y h_{cr}}{K_R - m_s h_{cr} g}. \quad [1.72]$$

Steady-state lateral load transfer

When the vehicle rolls, it results in a lateral shift of the vehicle COG due to the inertial force, and redistribution of the load between tires. Therefore, the inside wheels become unloaded and the outside becomes overloaded.

Summing the moments about the front and rear roll centers, the simplified steady-state equations of the lateral load transfer for the front and rear axles, ΔFz_F and ΔFz_R, respectively (assuming the roll acceleration $\ddot{\theta}$ and velocity $\dot{\theta}$ are equal to zero), are expressed as follows [MIL 95]:

$$\begin{aligned}\Delta Fz_F &= Fz_{11} - Fz_{12} \\ &= -2\frac{k_f}{e_f}\theta - 2m_s\frac{a_y}{l}\frac{l_r h_f}{e_f},\end{aligned} \quad [1.73]$$

$$\begin{aligned}\Delta Fz_R &= Fz_{21} - Fz_{22} \\ &= -2\frac{k_r}{e_r}\theta - 2m_s\frac{a_y}{l}\frac{l_f h_r}{e_r},\end{aligned} \quad [1.74]$$

where h_f and h_r are the heights of the front and rear roll centers, e_f and e_r the vehicle's front and rear tracks, k_f and k_r the front and rear roll stiffnesses, l_r and l_f the distances from the COG to the front and rear axles, respectively, and l the wheelbase ($l = l_r + l_f$) (see Figure 1.20).

Consequently, the front and rear total load transfer distributions, FLTD and RLTD, respectively, are given by:

$$\begin{aligned} \text{FLTD} &= \frac{\Delta F z_F}{\Delta F z_F + \Delta F z_R} \\ \text{RLTD} &= \frac{\Delta F z_R}{\Delta F z_F + \Delta F z_R} \end{aligned}. \quad [1.75]$$

Therefore, the lateral load transfer applied to the left-hand side of the vehicle is given by the dynamic relationship [1.76]:

$$\begin{aligned} \Delta F z_l &= (F z_{11} + F z_{21}) - (F z_{12} + F z_{22}) \\ &= -2(\frac{k_f}{e_f} + \frac{k_r}{e_r})\theta - 2m_s \frac{a_y}{l}(\frac{l_r h_f}{e_f} + \frac{l_f h_r}{e_r}). \end{aligned} \quad [1.76]$$

The lateral load transfer applied to the right-hand $\Delta F z_r$ is assumed equal to $-\Delta F z_l$. The lateral load transfer in [1.76] can be obtained by the summation of the following terms:

– $\Delta F z_{ge} = m_s \frac{a_y}{l}(\frac{l_r h_f}{e_f} + \frac{l_f h_r}{e_r})$, which is the geometric load transfer. This depends on the height of the roll centers.

– $\Delta F z_{el} = \theta(\frac{k_f}{e_f} + \frac{k_r}{e_r})$, which is the elastic load transfer, and is a function of the roll stiffness.

1.5. Summary

This chapter places an emphasis on the physical meaning of the vehicle dynamics. It covers the dynamic modeling of the vehicle/tire system.

The tire/road interactions are first described. Tire forces/moments are defined and consequently semi-empirical tire models are discussed. The quasi-static Pacejka's Magic tire formula, Dugoff's model and the linear model representing the tire behavior are presented and compared. The Magic formula is the most commonly used model. However, it requires a large number of tire-specific parameters that are usually unknown. Dugoff's tire model is not as accurate as the Magic formula, but it has the advantage of synthesizing the main tire properties into two parameters. The linear tire model is the simplest, but it overestimates the tire forces when the tire slip is significant and tire nonlinear zone is reached. The transient behavior of the tire is presented according to a relaxation tire model. Longitudinal and lateral tire–road friction are also interpreted.

Next, vehicle body dynamics are considered. Vertical, longitudinal, lateral and roll motions are modeled. As a basic condition, the different models are chosen to be

simple and sufficiently representative to be suitable for real-time applications. The quarter-car model is chosen to describe the vehicle's vertical movement. Longitudinal and lateral behaviors are represented using the FWVM, while the roll behavior is described using a roll plane model.

The vehicle/tire models presented will constitute the backbone for the vehicle-state estimator developed so far. The next chapter will explain the estimation concept and provide some observational tools and techniques.